

# Concentration driven cocrystallisation and percolation in all-cellulose nanocomposites

Denis Lourdin · Jorge Peixinho ·  
Joël Bréard · Bernard Cathala ·  
Eric Leroy · Benoît Duchemin

Received: 27 May 2015 / Accepted: 28 October 2015 / Published online: 7 November 2015  
© Springer Science+Business Media Dordrecht 2015

**Abstract** All-cellulose nanocomposites reinforced by cellulose nanocrystals (CNC) were produced using a solvent consisting of 1-butyl-3-methylimidazolium chloride and dimethyl sulfoxide. Microcrystalline cellulose (MCC) was pre-dissolved at high temperature in the solvent. Freeze-dried CNC were then added to the slurry at room temperature, thereby avoiding complete CNC dissolution. Solid all-cellulose composite films were obtained by film casting, solvent exchange and drying. The MCC to CNC ratio was kept constant while the solvent content was incremented. The short-range and long-range cellulose–cellulose interactions in the solid materials were respectively assessed by Fourier-transform infrared spectroscopy

and X-ray diffraction. The CNC used in this work contained both cellulose I and cellulose II. The cellulose concentration in the mixture drastically changed the overall crystallinity as well as the cellulose I to cellulose II ratio in the ACC. Cellulose II was formed by recrystallisation of the dissolved fractions. These fractions include the pre-dissolved MCC and the cellulose II portion of the CNC. Cocrystallisation with the cellulose I CNC acting as a template was also evidenced. This phenomenon was controlled by the initial solvent content. The correlation between the hygromechanical properties and the nanostructure features of the ACC was investigated by humidity-controlled dynamic mechanical analysis (RH-DMA). The introduction of the cocrystallisation and percolation concepts provided a thorough explanation for the humidity dependency of the storage modulus.

**Electronic supplementary material** The online version of this article (doi:10.1007/s10570-015-0805-x) contains supplementary material, which is available to authorized users.

D. Lourdin · B. Cathala  
UR1268 Biopolymères Interactions Assemblages, INRA,  
44300 Nantes, France

J. Peixinho · J. Bréard · B. Duchemin (✉)  
Laboratoire Ondes et Milieux Complexes, UMR 6294,  
CNRS-Université du Havre, 53 rue Prony, BP540,  
76058 Le Havre, France  
e-mail: benoit.professional@gmail.com;  
benoit.duchemin@univ-lehavre.fr

E. Leroy  
CNRS, GEPEA, UMR 6144, CRTT, LUNAM Université,  
37, Boulevard de l'Université, 44606 St Nazaire Cedex,  
France

**Keywords** Cellulose · Ionic liquid · Crystallization · Confinement · DMA

## Abbreviations

AFM	Atomic force microscopy
TEM	Transmission electron microscopy
FTIR	Fourier-transform infrared spectroscopy
WAXD	Wide-angle X-ray diffraction
RH-DMA	Humidity-controlled dynamic mechanical analysis
BmimCl	1-Butyl-3-methylimidazolium chloride
MCC	Microcrystalline cellulose

CNC	Cellulose nanocrystals
DMSO	Dimethyl sulfoxide
ACC	All-cellulose composites
RCF	Regenerated cellulose film
LOI	Lateral order index
TCI	Total crystallinity index

## Introduction

All-cellulose composites (ACC) are mono-component materials in which strong and stiff cellulose crystallites are embedded in a cellulose matrix. These composites are generally obtained by heterogeneous (or partial) dissolution of cellulose, followed by a controlled precipitation to form a bulk material. In a way, they can actually be considered as a new take on older products such as parchment, tracing, vulcanised and gelatinised papers (Bras 2004; Cartier et al. 1994; Nishino et al. 2004; Schmidt 1871). Vulcanised and gelatinised paper came before cellophane. They were very important materials economically from the second half of the 19th century until the advent of artificial and synthetic polymers in the early 20th century. These two types of papers were of particular interest due to their excellent thermo-mechanical and electrical insulation properties. Both could also be plasticised in order to manufacture a material with “flexibility (...) resembling soft vulcanised rubber” (Schmidt 1871). Furthermore, gelatinised paper could be moulded into complex shapes as detailed in the original patent of Courtenay filed in 1878 (Courtenay 1878). Environmental issues were probably not as important as they are today but these materials should have preserved the original biodegradability of cellulose; additionally, they were recyclable (Courtenay 1878; Kalka et al. 2014). The term “all-cellulose composites” was first introduced by Nishino et al. (2004) as a reference to all-polymer composites such as all-poly (ethylene) composites (Nishino et al. 2004). The introduction of a new term to designate an old material translates the rupture that has taken place when studying a 19th century engineering achievement with modern scientific tools. Since vulcanised and gelatinised paper saw their rise and decline before the advent of modern spectroscopy and microscopy techniques, a vast potential of understanding and improvement is offered to the modern

scientist. The renewed academic interest for this class of materials is illustrated by a relatively vast body of literature published on this topic over the last decade (Duchemin et al. 2007, 2009a, 2010; Gindl and Keckes 2005; Haverhals et al. 2012, 2010; Huber et al. 2012; Nishino et al. 2004; Nishino and Arimoto 2005; Ouajai and Shanks 2009; Pullawan et al. 2012, 2014; Soykeabkaew et al. 2008, 2009a). This modern effort can doubtlessly be a vast source of improvement to help making these composites more environmentally-friendly, more functional or simply tougher.

Several interesting facts have recently emerged from detailed spectroscopic and analytical studies. When ACC are produced by heterogeneous or partial dissolution, an absence of allomorphic swap from cellulose I to cellulose II was observed in the early stages of cellulose dissolution. Dissolution was however evidenced by satisfactory inter-particle bonding and thorough microstructural changes (Duchemin et al. 2007; Soykeabkaew et al. 2009b). Furthermore, it is possible to reconsolidate a material with a near absence of crystallinity loss when the ratio of polymer to solvent is high, when the precipitation is kinetically favourable or when an important specific surface area of the cellulosic material is exposed to the solvent (Duchemin et al. 2007, 2009b; Soykeabkaew et al. 2009b). The high crystallinity of these materials can probably be attributed to the absence of coiling of the polymer chains due to the confinement between undissolved, solid particles. ACC can also be produced by a different method involving mixing a solid template in a pre-dissolved cellulose slurry (Buleon et al. 1976, 1977; Buleon and Chanzy 1980; Huber et al. 2012; Nishino et al. 2004; Pullawan et al. 2014). The regenerated material is then found into confined spaces delimited by the solid particles. Its crystallization in the form of cellulose IV<sub>II</sub> or cellulose II means that the polymer chains in solution uncoiled in these spaces and packed longitudinally according to the crystal lattice formed. Adding a bit of complexity to the system, the undissolved cellulose template and the polymer in solution can interact. If the undissolved template is found in the form of nanoparticles with a large surface area, the surface interaction could become prevalent and templated epitaxial growth has been observed (Buleon et al. 1976, 1977; Buleon and Chanzy 1980; Ma et al. 2011; Pullawan et al. 2010, 2014). When cellulose is in its non-derivatised form, it is clear that the interaction comes in the form

of physical crosslinks that are triggered by gelation (Wang and Chen 2010). These physical crosslinks are at the origin of the interface between matrix and reinforcement in the dried regenerated composites. In order to quantify the efficiency of this interface, the shift of a peak assigned to the C–O stretch mode along the cellulose backbone was measured by Raman spectroscopy on strained specimens of model ACC in which the crystalline domains are well defined cellulose nanocrystals (CNC) (Pullawan et al. 2010, 2012, 2014). The stress transfer from the matrix to the CNC occurred systematically. This results in an efficient reinforcement effect, with a stiffness increase proportional to the relative amount of CNCs even though Young's modulus and tensile strength reach threshold values at high CNC content (Pullawan et al. 2014; Qi et al. 2009). The above structure property relationships indirectly point out the crucial role played by the production processes of the ACC. Many variations have been investigated, in which the initial cellulose sources and the solvent used are key parameters.

The recent developments of ACC are driven by the use of less toxic, biobased, biodegradable and more efficient solvents. Indeed, usual cellulose solvents are often plagued by their low efficiency, detrimental effect on molecular weight, price, toxicity, corrosiveness, uneasy use in industrial conditions with high temperatures, toxic by-products and risks of thermal runaway (Boerstoel 2006; Duchemin 2008; Liebert 2010). In the last decades, a few interesting solvents have emerged. The use of mixtures of orthophosphoric acid have been proved to form liquid crystalline phases that could be used some of the strongest man-made fibres with a tensile strength as high as 1.7 GPa (Boerstoel 2006). Ionic liquids have also interesting properties in that they can be recycled and can dissolve cellulose in large concentrations. Ionic liquids can for example be used for the production of textile fibres, ACC and thin films with or without atypical cellulose spherulite formation (Graenacher 1934; Huber et al. 2012; Song et al. 2013; Zhu et al. 2006). Ionic liquids can be mixed in small fractions with organic co-solvents in order to reduce the viscosity of highly concentrated cellulose dopes (Rinaldi 2011; Wang et al. 2014). This viscosity decrease is industrially favourable in that it facilitates the forming of regenerated objects (Fink et al. 2014; Pinkert et al. 2010; Röder et al. 2009).

Regarding the cellulose sources, while regenerated cellulose fabrics are preferred in upscaling approaches in order to produce thick composite parts, the above mentioned CNC-reinforced ACC open perspectives for designed nanocomposite materials (He et al. 2014; Ma et al. 2011; Olszewska et al. 2013; Pullawan et al. 2010, 2012, 2013, 2014; Qi et al. 2009; Wang and Chen 2010). In this article, a focus is made on model systems. The objective will be to study the influence of the total cellulose content (CNC and dissolved cellulose) in the solvent on the formation of the ACC's structure. This implies specific choices regarding both the CNC source and the concentrations to be studied. To the best of our knowledge, all published works used a cellulose I CNC source. In many cases, the CNC were added in the form of a suspension in the pre-dissolved matrix (He et al. 2014; Ma et al. 2011; Qi et al. 2009). As a consequence, two parameters were changed at once: the CNC to dissolved polymer ratio and the hydrodynamic volume occupied by the CNC. In the present work, an opposite approach was taken where a mixture of freeze-dried CNC composed of cellulose I and cellulose II was added to the pre-dissolved cellulose solution. The solvent was a mixture of an imidazolium-based ionic liquid with DMSO. The relative amount of CNC and pre-dissolved cellulose was kept equal in order to elucidate the effect of the hydrodynamic volume occupied by the templates on the matrix recrystallisation and on the microstructure of the composites. This confinement effect was studied using atomic force microscopy (AFM), transmission electron microscopy (TEM), Fourier-transform infrared spectroscopy (FTIR), wide-angle X-ray diffraction (WAXD) and humidity-controlled dynamic mechanical analysis (RH-DMA).

## Materials and methods

### Materials

Cellulose nanocrystals (0.95 wt% sulfur on CNC sodium form,  $\zeta = -63.7 \pm 2.6$  mV, surface charges measured to  $0.128$  e/nm<sup>2</sup>) were obtained from Le Maine University in the form of a suspension with a 7.08 wt% solid content. Quartz (>99 %, Roth, ref 4651.1) with a particle size >125  $\mu$ m was used as a preparatory aid for CNC characterization by WAXD. The 4 Å molecular sieve (Roth, ref 8471.2), the

1-butyl-3-methylimidazolium chloride (BmimCl,  $\geq 95\%$ , Aldrich, ref 38899-100 ml) and the microcrystalline cellulose (MCC, Avicel®, Macherey–Nagel, ref 815290.1, DP  $\sim 40$ –200) were all dried in a vacuum oven at  $103\text{ }^{\circ}\text{C}$  for at least 48 h prior to use. The viscosity of the cellulose solution was lowered with dimethyl sulfoxide (DMSO,  $\geq 99.5\%$ , Sigma ref D4540-500 ml).

### Preparation

The molecular sieve was added to the DMSO for drying prior further use. 20 g of solution were prepared by varying the total cellulose content from 1 to 8 wt% and by keeping the MCC to CNC weight ratio to a fixed value of 1:1. A 1:1 DMSO:BmimCl weight ratio was maintained throughout the experiments. In a first step, the pre-dried MCC and DMSO were mixed together and stirred for 5 min in order to form a homogeneous suspension, thereby facilitating further dissolution. A weighted amount of BmimCl was then added to the suspension and mixed for 5 min. The suspension was then re-heated for 5 min at  $103\text{ }^{\circ}\text{C}$  and stirred to achieve complete dissolution. A sealed glass bottle and a magnetic stirrer were used in order to reduce the exposure of the solution to moisture. The solution then appeared visually transparent and devoid of lumps. After this step was completed, a given amount of freeze-dried CNC was added to the mixture which was immediately sealed and left for stirring for 15 days at room temperature. The samples were then cast on glass Petri dishes and left for equilibrium for 24 h. They were then placed in a sealed box with a humidity-saturated atmosphere at room temperature for 24 h before being immersed in an excess of distilled water. The samples were then transferred to a water bath for 3 days and the water was exchanged once a day. The resulting hydrogels were then dried by exposure to room air at room temperature in their Petri dish for at least 48 h. The films will be called ACC1, ACC2, ACC4, ACC6 or ACC8 depending on the total amount of cellulose in the initial mixture (Table 1). A regenerated cellulose film (RCF) comprising 4 wt% MCC without CNC was also prepared.

### Measurements

TEM was performed under standard conditions using a JEOL JEM-1230 TEM at 80 kV. The samples were

prepared as follows: 20  $\mu\text{l}$  of a cellulose nanocrystals suspension in water (0.1 % w/v) was deposited on a freshly glow-discharged carbon-coated copper grid (Electron Microscopy Sciences, UK) for 2 min, and the excess was removed by blotting. Negative staining was immediately performed using 20  $\mu\text{l}$  of phosphotungstic acid (1 % w/v, adjusted to pH 6 with NaOH) for 2 min and the excess solution was blotted before drying grids at room temperature.

AFM was conducted on a Bruker Innova. The CNC suspension was diluted with distilled and filtered water to 0.24 % solid weight before being deposited on a mica substrate and dried in liquid nitrogen flow. They were then imaged in contact mode with a TESPATIP (320 kHz, 20–80 N/m).

WAXD was performed in the reflection mode using a “gonio scan” ( $\theta$ – $\theta$ ) on a Pan’alytical X’pert powder diffractometer equipped with a  $\text{CoK}\alpha$  anode ( $\lambda = 1.7903\text{ \AA}$ ) powered at 40 kV and 40 mA. Programmable anti-scatter slits had a fixed aperture of  $1/4^{\circ}$  whereas the anti-diffusion slits had an aperture of  $1/2^{\circ}$ . A 5 mm mask was selected. The detector was a linear Pix’cel 1D detector equipped with 0.04 rad Soller slits. The scan was performed in the  $5$ – $50^{\circ}$  range in steps of  $0.05^{\circ}$  (2000 s/step). The ACC were measured on a flat sample holder. The CNC was measured with a slightly different procedure in order to produce a satisfactory powder scan: the suspension was mixed with a quartz powder (7 wt% based on the dry extract) before being hand-crushed into a fine powder in a mortar-and-pestle. All samples were continuously spun at 7.5 rpm along the phi direction during measurement. The quartz signal was subtracted from the spectra before data processing with respect to its (101) peak intensity. The curves were then area normalized before being fitted with a model comprising the (1 $\bar{1}$ 0), (110), (102), (200) and (004) Gaussian contributions from cellulose I, the (1 $\bar{1}$ 0), (110), (020) Gaussian contributions from cellulose II and a non-crystalline semi-empirical background as described elsewhere (Duchemin et al. 2012).

FTIR measurements were done directly on the films with a Perkin Elmer Frontier spectrometer equipped with a diamond attenuated total reflectance accessory. The data was averaged over 16 runs with a resolution of  $2\text{ cm}^{-1}$  in the  $4000$ – $650\text{ cm}^{-1}$  region and at least three measurements were performed for each sample. Calculations of the total crystallinity index (TCI) was performed from the ratio of the absorption peaks

**Table 1** Composition of the solutions and suspensions prepared in this work prior precipitation and drying to form the solid films

Sample name	CNC content (wt%)	MCC content (wt%)	DMSO:BmimCl (1:1) content (wt%)
RCF	0	4	96
ACC1	0.5	0.5	99
ACC2	1	1	98
ACC4	2	2	96
ACC6	3	3	94
ACC8	4	4	92

1372/2900  $\text{cm}^{-1}$  (Carillo et al. 2004; Nelson and O'Connor 1964a). The strongest band of the three bands at 2900  $\text{cm}^{-1}$  was chosen. The lateral order index (LOI) (1420/893  $\text{cm}^{-1}$ ) was also determined.

RH-DMA measurements were done on a Metravib DMA 50. The tensile mode was used at a frequency of 1 Hz, with a deformation amplitude of 0.01 % which is in the range of linear viscoelasticity. Measurements were performed on a piece of film about  $5 \times 15$  mm and a thickness from 40 to 50  $\mu\text{m}$ . Simultaneously to the dynamic solicitation, a static force of 0.5 N was applied in order to maintain the film in tension. Storage and loss modulus were measured under controlled atmosphere from about 5 to 95 % relative humidity. The humidity was obtained by mixing a dry air flow with a water saturated air flow, thermostated by a circulating water bath at 22 °C. The measurement temperature was kept constant at  $22 \pm 1$  °C and the relative humidity was also measured using a humidity sensor close to the sample.

## Results

### Atomic force microscopy and transmission electron microscopy

The average CNC dimensions were measured using AFM and TEM (Fig. 1). The goal of this measurement was to assess whether the crystallites were well individualized by comparison with XRD results. Due to tip broadening and lateral aggregation on the substrate, AFM was solely used to measure the CNC thickness whereas TEM was used to give an estimate of the CNC length and width. These commercial nanocrystals had a length  $106 \pm 41$  nm, a width of  $15 \pm 5$  nm and a thickness of  $5 \pm 1$  nm. Their width

could appear slightly exaggerated. It can however be explained by their tendency to pack laterally against the TEM grid upon drying. These results are all in good agreement with recently published results for commercial CNC produced from wood pulp (Boluk et al. 2011; Lu et al. 2014).

### X-ray diffraction

The CNC are peculiar in that they contain both native cellulose I and cellulose II (Fig. 2). A simple peak fitting procedure shows that the (1 $\bar{1}$ 0), (110), (102), (200) and (004) peaks of cellulose I have interplanar spacings of 5.99, 5.34, 4.35, 3.9, 2.60 Å; the (1 $\bar{1}$ 0), (110) and (020) peaks of cellulose II have interplanar spacings of 7.21, 4.44 and 4.03 Å, in accordance with the literature for both allomorphs (Buleon et al. 1977; Isogai 1989; Newman 2008; Takahashi and Ookubo 1993). According to the peak fitting procedure, cellulose I amounted to  $\sim 59$  % of the crystalline content. A slightly higher value of 72 wt% was found using a Rietveld analysis in the software Maud (data not shown here). Mixtures of coexisting nanocrystals of cellulose I and cellulose II have already been observed in some other works (Sèbe et al. 2012). Strikingly, the lateral size of the cellulose II crystallites is fairly large: their thickness of 44–49 Å (Table 2) is similar to the size measured by AFM and to sizes measured on regenerated or mercerized cellulose materials (Boerstoel 2006; Smole et al. 2003). Therefore, it is assumed that the CNC suspension contains entire crystallites of cellulose I and cellulose II. The total crystalline content as measured by peak fitting amounts to 27 %. If the sample was solely made of cellulose I, the corresponding crystallinity index as measured by Segal's method would amount to about 63 % (Duchemin et al. 2012; Segal

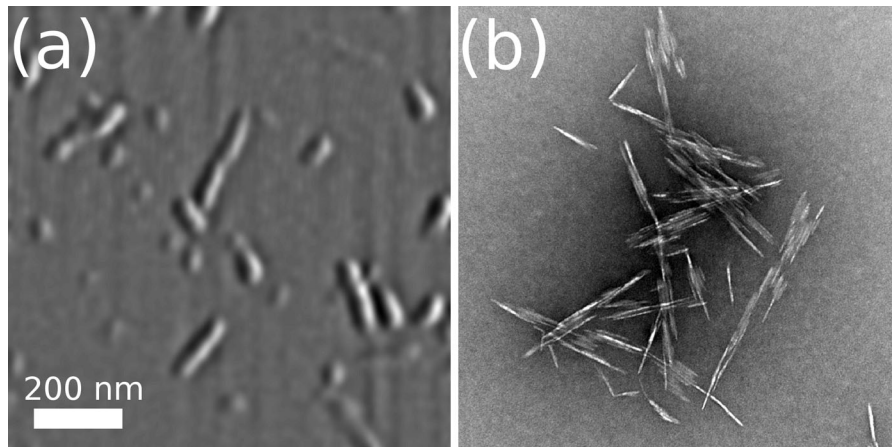


**Fig. 1** Atomic force microscope topography image (a) and transmission electron microscope micrograph (b) of as-received CNC at the same magnification

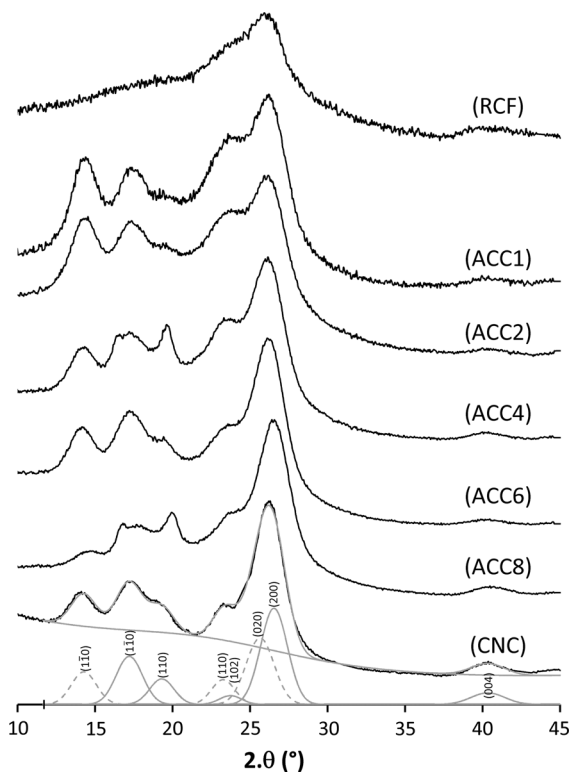


**Fig. 2** X-ray diffractograms of (top to bottom): RCF, ACC1, ACC2, ACC4, ACC6, ACC8 and CNC. The grey lines correspond to the peaks fitted to the CNC graph (plain lines: cellulose I; dotted lines: cellulose II). The diffraction planes are labeled above each peak

et al. 1959). This value is a bit lower than what is expected for a purely crystalline material, but it could be attributed to the cellulose I → cellulose II

conversion during the manufacturing process which creates more paracrystalline domains.

The RCF is very different in that it contains no cellulose I (Fig. 2). The RCF diffractogram has a broad maximum at  $25.97^\circ$  and a shoulder at  $23.10^\circ$  corresponding to interplanar distances of 3.98 and 4.47 Å, which is consistent with the (110) and (020) peaks of cellulose II. A slightly textured and low crystallinity cellulose II is also known to result in a spectrum in which these two peaks strongly overlap and in which the  $(1\bar{1}0)$  peak is not or poorly resolved (Duchemin et al. 2007; Goldberg et al. 2015; Smole et al. 2003).

The ACC were prepared by mixing an equal amount of CNC and MCC in the solvent at room temperature. These conditions are expected to promote little to no further dissolution of the solid CNC template (Ma et al. 2011; Pullawan et al. 2010, 2014). The resulting diffractograms were thus expected to be a weighted average of those obtained with RCF and CNC.

However, this was not the case. Mixing CNC with the cellulose slurry yielded a fair amount of nonlinear changes in the allomorphic composition. The most noticeable change is the higher total amount of cellulose II in ACC1 when compared to both the original CNC and RCF and the much lower amount of cellulose II in ACC8, the composite prepared with the highest initial cellulose concentration of cellulose (Fig. 3). Of all the composites, ACC1 had the smallest cellulose II crystallites, with a size perpendicular to the (020) diffraction plane similar to that determined

**Table 2** Lateral crystallite sizes as determined by XRD peak fitting

Sample name	Cellulose I size along (200) (Å)	Cellulose II size along (020) (Å)	Cellulose II size along (1 $\bar{1}$ 0) (Å)	Ratio cellulose II/crystalline material
RCF	n.a.	29	Could not be determined	1
CNC	46	44	49	0.41
ACC1	41	28	41	0.61
ACC2	41	42	44	0.54
ACC4	43	49	53	0.45
ACC6	46	49	47	0.45
ACC8	40	42	42	0.11

in RCF (Table 2). Paradoxically, this sample also had the highest crystallinity of all samples (Fig. 3). In contrast, ACC8 had the lowest crystallinity of all ACC and virtually no cellulose II left. As the initial cellulose concentration in the ACC increased, the relative amount of cellulose II decreased (Table 2). The size and content of cellulose I evolved little in all composites. The cellulose I crystallites were however on average 9 % more slender than the initial ones found in CNC, suggesting surface re-arrangement of the cellulose I templates after composite consolidation. Finally, a mention should be made about the peculiar aspect of the (110) peak of cellulose I found in the ACC of highest concentration (ACC4 to ACC8). This peak is fairly sharp which often indicates a pronounced crystallographic texture.

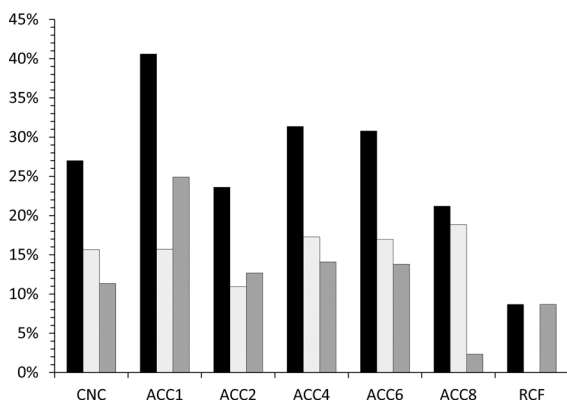


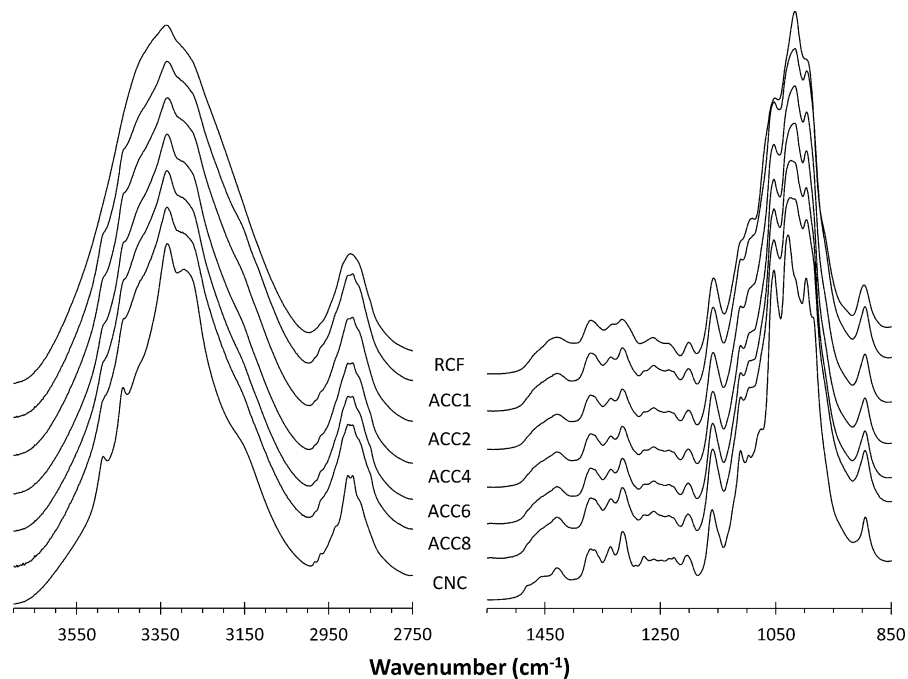
**Fig. 3** Crystallinity (black), cellulose I (light grey) and cellulose II (dark grey) weight percents of the various specimens determined by XRD. The correlation coefficient between measured data and model was always >0.998

## FTIR

### Allomorphy

Figure 4 displays the FTIR spectra of the ACC samples compared to those of RCF and CNC. The peaks at 1335 and 1315  $\text{cm}^{-1}$  are respectively assigned to  $-\text{OH}$  in-plane bending and to  $\text{CH}_2$  wagging motion (Carillo et al. 2004; Nelson and O'Connor 1964b; Schwanninger et al. 2004). When cellulose is made amorphous by ball-milling, these peaks flatten and merge (Nelson and O'Connor 1964b; Schwanninger et al. 2004). In the present work, these peaks were visible on all spectra confirming the presence of crystalline cellulose I or cellulose II (Fig. 4). They were very sharp in the CNC spectra. On the contrary, they were the least sharp in the RCF sample. In the ACC, they tended to flatten with a decreasing polymer concentration. In the same manner, the peak at 1429.5–1429  $\text{cm}^{-1}$  became broader following the order  $\text{CNC} < \text{ACC8} < \text{ACC6} < \text{ACC4} < \text{ACC2} \leq \text{ACC1} < \text{RCF}$ . This peak is attributed to  $\text{CH}_2$  symmetric bending or scissoring motion. Its magnitude decrease is consistent with a change in the environment of the C(6) group, which is itself consistent with a transition to a material containing less cellulose I (Carillo et al. 2004; Kondo and Sawatari 1996; Nelson and O'Connor 1964a, b; Oh et al. 2005a, b). A similar conclusion could be drawn from the peak near 1110  $\text{cm}^{-1}$  which is attributed to the ring asymmetric stretching and which is known to be a sum of cellulose I peak at 1111  $\text{cm}^{-1}$  and of a cellulose II peak at 1007  $\text{cm}^{-1}$  (Carillo et al. 2004).

**Fig. 4** FTIR spectra in transmittance of the samples in the following order (*top to bottom*): RCF, ACC1, ACC2, ACC4, ACC6, ACC8 and CNC



The materials also showed significant differences in the  $\text{-CH}$  stretching region between  $3000$  and  $2850\text{ cm}^{-1}$  (Fig. 4). This region is known to contain several bands of interest (Altaner et al. 2014; Carillo et al. 2004; Schwanninger et al. 2004; Sukhov et al. 1998; Zugenmaier 2001). The two bands at  $2920$  and  $2850\text{ cm}^{-1}$  are assigned to the ring  $\text{-CH}$  of crystalline cellulose I and II and they are polarised perpendicularly to the polymer chain axis. Another band at  $2890\text{--}2905\text{ cm}^{-1}$  is found in cellulose I, cellulose II and amorphous cellulose. This band is assigned to the C(6) vibration of the hydroxymethyl group. It is thus fairly sensitive to the changes of environment in the hydrogen bonding pattern such as the changes undergone during allomorphic conversion or decrystallisation. Cellulose  $\text{I}_\beta$  usually produces a spectrum with a single maxima at around  $2902\text{ cm}^{-1}$ . The complete conversion of cellulose  $\text{I}_\beta$  to cellulose II shifts this peak to a lower wavenumber near  $2892\text{ cm}^{-1}$  (Carillo et al. 2004; O'Connor et al. 1958; Oh et al. 2005a, b; Schwanninger et al. 2004). When cellulose is decrystallized by ball-milling, the main peak at  $\sim 2900\text{ cm}^{-1}$  is also shifted to lower values; extensive decrystallisation produces a broader  $\text{-CH}$  region with a double peak at  $2892$  and  $2921\text{ cm}^{-1}$  (Duchemin 2008; Kondo and Sawatari 1996; Schwanninger et al.

2004). The ACC spectra exhibited two local maxima at  $2904$  and  $2893\text{ cm}^{-1}$ . The presence of crystalline cellulose I was thus obvious in all spectra but in the RCF one, which is the sole one comprised solely of cellulose II. The  $\text{-CH}$  region maximum for the samples ACC6, ACC8 and CNC was found at  $2904\text{ cm}^{-1}$ , whereas that of the other composites was found at  $2893\text{ cm}^{-1}$ . This data indicates the simultaneous presence of both crystalline cellulose I and II in all ACC as well as in the CNC. They also show that the ACC with the highest initial cellulose concentration contained relatively more cellulose I than cellulose II.

The hydroxyl region also contains useful information. The main peak at  $3350\text{--}3330\text{ cm}^{-1}$  is attributed to intramolecular hydrogen bonds  $\text{O(3)H}\cdots\text{O(5)}$  parallel to the  $\beta$  1–4 glycosidic bond. The peak at  $3440\text{--}3450\text{ cm}^{-1}$  belongs to the C(2)O(2)H alcohol in native cellulose (Maréchal and Chanzy 2000; Oh et al. 2005a, b). Thanks to selective deuteration, it was also shown that the band at  $3440\text{ cm}^{-1}$  is assigned to accessible cellulose surface chains in native cellulose which are weakly hydrogen bonded (Fernandes et al. 2011; Maréchal and Chanzy 2000). It is known that a progressive transformation of cellulose I to cellulose II by NaOH treatment shifts the hydroxyl maximum



from  $\sim 3340$  to  $3440\text{ cm}^{-1}$ . A similar effect is induced by ball-milling, presumably by a progressive increase of the cellulose surface chains, which are known to display a different hydrogen pattern to that of internal chains located within the crystallites (Schwanninger et al. 2004). It is thus expected that an increasing cellulose II/crystalline material ratio yields a stronger  $3440\text{ cm}^{-1}$  band in accordance with XRD results, which is actually observed here when comparing CNC and RCF (Figs. 4, 5). The variation of this relative band intensity is less easy to explain for the ACC (Fig. 5). At first, it undergoes a clear decrease between ACC1 and ACC4. This decrease correlates well with the decrease in cellulose II content, as observed previously. However, the change in relative values seems to remain steady (within margin of error) between ACC4 and ACC8. Since it was observed that the cellulose II content continually decreases over this concentration window as well, the strength of the signal of the surface chains at  $3440\text{ cm}^{-1}$  must be increased by the production of a non-crystalline material.

The lateral order index (LOI) is the ratio of the band at  $1430\text{ cm}^{-1}$  to the band near  $895\text{ cm}^{-1}$ . The band at  $1430\text{ cm}^{-1}$  is described above and it is known to be very sensitive to changes of conformation. On the contrary, the band in the fingerprint region near  $890\text{ cm}^{-1}$  is attributed to C(1) vibrations, a vibration that is little affected by allomorphic transformations or decrystallisation. This index was first reported by O'Connor et al. (1958) as a measure of cellulose crystallinity (O'Connor et al. 1958). It was later named LOI by Hurtubise and Krassig (1960). The LOI

increases with the crystallinity of cellulose I and decreases with an increasing crystallinity of cellulose II (Nelson and O'Connor 1964a). In general, if cellulose I and cellulose II with similar accessibility, i.e. surface chains, coexist, then the LOI will be lower for cellulose II (Hurtubise and Krassig 1960; Nelson and O'Connor 1964a). Similar observations were performed by O'Connor et al. (1958) by mixing cellulose I and cellulose II in various proportions (O'Connor et al. 1958). It was shown that a decreasing LOI was observed for a native cellulose transformed to regenerated cellulose by progressive mercerisation, and that this change was relatively unrelated to the crystallinity as measured by XRD (Hurtubise and Krassig 1960; Oh et al. 2005b). The LOI observed here was lower for the fully dissolved film (RCF) than for the CNC. Importantly, the ACC underwent a steady increase of their LOI with an increase in their initial polymer concentration (Fig. 6). Whereas the composites with the lowest concentration had the lowest LOI of all samples, ACC8 had a LOI similar to that of CNC. This trend can be explained by the higher relative cellulose I content of the ACC with the highest cellulose concentration.

### Crystallinity

Since the LOI bottleneck lies in its incapacity to deconvolute crystallinity and allomorphic changes, Nelson and O'Connor (1964a, b) proposed another index (the TCI) based on the use of the  $1372\text{ cm}^{-1}$  ( $-\text{CH}$  bending) peak which is present in all cellulose types and which seems fairly insensitive to changes in

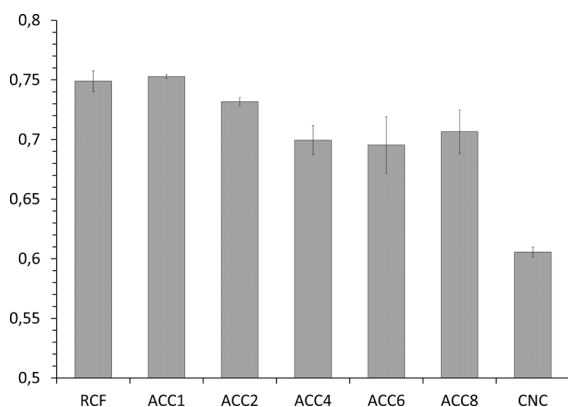


**Fig. 5** FTIR relative peak intensity of the shoulder at  $3440\text{ cm}^{-1}$  relative to the local maximum near  $3333\text{ cm}^{-1}$

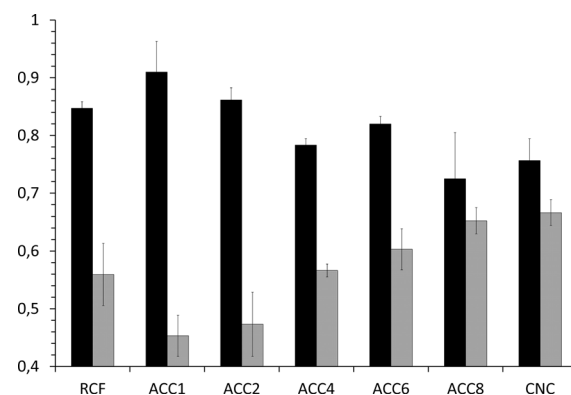


**Fig. 6** Total crystallinity index (black) and lateral order index (grey) as determined from FTIR data

allomorphic transformations (Nelson and O'Connor 1964a). The peak selected to reflect changes in crystallinity was the  $2900\text{ cm}^{-1}$  one detailed above. The TCI plot clearly shows a decrease in crystallinity of the composites with an increasing polymer concentration and the crystallinity of the sample prepared with the maximum amount of polymer (ACC8) has a lower crystallinity than the CNC (Fig. 6). This last result is in good agreement with the XRD results and with the low cellulose II content in particular. This phenomenon has also been observed for a regenerated cellulose fibre reinforced with cellulose I CNC (Magalhães et al. 2009). It has been suggested that the addition of CNC in a cellulose matrix could disturb the formation of hydrogen bonds in the regenerated material (Wang and Chen 2010). Nevertheless, the RCF sample has a fairly high crystallinity according to this method. This sample is the only one that doesn't comprise crystalline cellulose I. Consequently, the method has to be affected by other factors such as baseline placement. The peaks at  $1315$  and  $1270\text{ cm}^{-1}$  are attributed to in- and out-of-plane  $\text{-CH}$  bending and they are highly sensitive to the type of allomorph and to crystallinity (Carillo et al. 2004; Maréchal and Chanzy 2000; Nelson and O'Connor 1964a, b). Due to the absence of native cellulose in the RCF sample, these two bands could have affected the baselines drawn to determine the intensity of the peak at  $1372\text{ cm}^{-1}$  and introduced a bias in the TCI. Furthermore, FTIR measures a different crystallinity to XRD in that FTIR provides information on short range molecular order (Koenig 1999).

#### Humidity-controlled dynamic mechanical analysis

ACC8 was too brittle to be tested in the RH-DMA. It is indeed well-known that the strain-to-failure of ACC decreases with an increasing CNC content and so the rest of the discussion will be purported to the composites that could be tested (Pullawan et al. 2014). Of all the films, the CNC films exhibited the largest storage modulus at  $\sim 9\text{ GPa}$  near 5–10 % RH. This modulus was largely affected by the moisture content and it dropped steadily by 7 GPa when the relative humidity reached 95 %. In contrast, the RCF had a fairly low storage modulus of  $\sim 2.5\text{ GPa}$  up until 40 % RH, which is well in-line with literature values (Zhou et al. 2001). This modulus dropped to  $\sim 0.9\text{ GPa}$  at 95 % RH, which corresponds to a

$\sim 1.6\text{ GPa}$  decrease. The ACC had intermediary properties. ACC1 had a behaviour near that of the RCF. Overall, the other ACC had a storage modulus getting gradually closer to that of the CNC film as their initial cellulose concentration was increased (Fig. 7).

Water is a well-known plasticiser for regenerated cellulose films (Mazeau 2015; Salmén and Back 1977; Zhou et al. 2001). The accessible cellulose chains can bind to water molecules. In turn, these water molecules disrupt the intermolecular hydrogen bonds that provide stiffness to the dry material and act as plasticisers. There are just a few examples in the literature where humidity-controlled dynamic mechanical testing was used to probe differences in regenerated cellulosic materials (Sundberg et al. 2013; Zhou et al. 2001). It was observed that the storage modulus of regenerated cellulose start dropping dramatically at about 70–80 % RH, which is the case in the present work. This plasticization is probably due to the proximity of the  $\alpha_3$  viscoelastic relaxation (Duchemin 2008; Manabe et al. 1986; Nissan and Sternstein 1962). Water also disrupts the hydrogen bonds of *geometrically* percolated CNC networks in CNC films and in their composites (Capadona et al. 2008; Pullawan et al. 2013). As a consequence, the CNC films undergo a large storage modulus drop when exposed to humidity in spite of their high crystallinity. This storage modulus drop is more than four times the one observed for regenerated cellulose films (Zhou et al. 2001).

In the present work, a higher initial cellulose concentrations in the ACC meant a higher dry storage

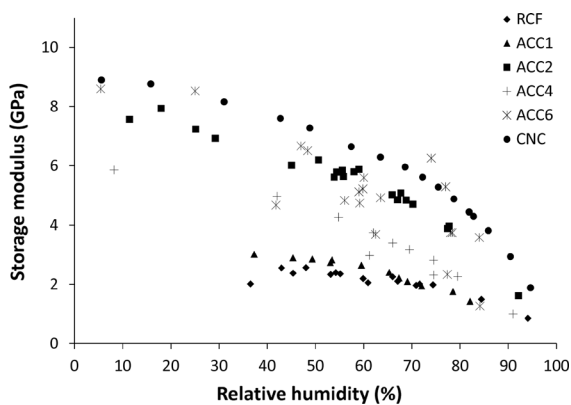


**Fig. 7** Storage modulus  $E'$  as a function of humidity of RCF (diamond), ACC1 (triangle), ACC2 (square), ACC4 (plus), ACC6 (asterisk) and CNC (circle)

modulus and a larger susceptibility to water plasticisation. Whereas the latter could be explained both by the plasticisation of the amorphous cellulose matrix or by that of a percolated CNC network, the former can only be explained by the formation of a stiff, long-range, percolated CNC network. The hygromechanical behavior of the ACC is thus very similar to that of the CNC film: ACC2 and ACC6 undergo a large drop in storage modulus about one order of magnitude upon humidity exposure. Therefore, CNC percolation dominates the dynamic hygromechanical behavior of the composites that have the higher initial cellulose concentrations. The wet storage modulus of the composites containing percolated CNC is however essentially that of the matrix: the CNC–CNC interactions are “switched-off” at high humidity. This can explain the convergence of modulus of all ACC films at high humidity. Furthermore, whereas the CNC film immersed in water tended to turn back into a paste, the RCF and the ACC were softened but remained solid (data not shown here). Hence, the hygromechanical behaviour of the ACC is truly intermediary between that of the RCF and that of the CNC film.

A micromechanical model exists to describe the mechanical behavior of percolated CNC (Capadona et al. 2008; Flandin et al. 2000). This model is an adaptation of the model described by Takayanagi et al. (1964) for semi-crystalline polymers in order to account for the high aspect ratio of the reinforcement (Takayanagi et al. 1964). It also accounts for the percolation behaviour which is not well described by the Halpin-Kardos model for isotropic short fibre composites. In our case, the percolation model was fitted to the data with a good level of accuracy and a correlation coefficient always superior to 0.98. Based on the percolation assumption, the model unambiguously shows that an increasing CNC volume fraction contributes the storage modulus as the initial cellulose concentration is increased in the slurry (see Supporting information).

## Discussion

Both XRD and FTIR underline the important function of the initial concentration of cellulose in the mixture. This concentration plays a decisive role on the cellulose II content as well as on the crystallinity. Whereas the cellulose I content is relatively unaffected

during composite manufacturing, the cellulose II ratio changes in drastic proportions. Cellulose II is almost absent in ACC8. This absence suggests that the cellulose II nanocrystals were dissolved in the solvent. Since dissolution is kinetically more effective at lower concentrations, it is inferred that the cellulose II nanocrystals were in fact always dissolved in the DMSO:BmimCl mixture and regenerated later as part of what is understood to form the matrix.

In contrast, cellulose II is present in large quantities in the ACC produced with the lowest initial cellulose concentrations and these quantities are much larger than what would be expected if the rule of mixtures was applied. TCI and crystallinity as measured by XRD also increase with the cellulose II content. This variation strongly suggests that cellulose II cocrystallised in the presence of native CNC. Wang and Chen (2010) have evidenced by rheology the physical crosslinking taking place during gelation between the cellulose chains in solution and the solid CNC in suspension (Wang and Cheng 2009). This crosslinking is an indication of the polymer adsorption on the nanoparticles and its extent was found to increase with an increasing CNC content. After the dissolved cellulose chains are adsorbed on the native cellulose template, cellulose II cocrystallisation can occur (Buleon et al. 1976, 1977; Buleon and Chanzy 1980; Magalhães et al. 2009; Pullawan et al. 2014). In particular, Buléon et al. demonstrated in a series of papers using a crystalline cellulose extracted from the cell wall *Valonia ventricosa* (a cellulose containing typically 64 %  $I_{\alpha}$  and 36 %  $I_{\beta}$  crystallites) the possibility for a native cellulose template to promote the nucleation and the epitaxial growth of a low DP regenerated cellulose in a shish-kebab structure (Buleon et al. 1976, 1977; Buleon and Chanzy 1980; Imai and Sugiyama 1998). However, this cocrystallisation is known to be limited to cases where the relative amount of template remains low (Buleon et al. 1976; Magalhães et al. 2009; Pullawan et al. 2014).

In the present case, a decrease (or a plateau) of crystallinity is observed when the CNC are present in relatively large quantities. This decrease is correlated with a near absence of cellulose II. In place of cellulose II, the matrix is richer in a material akin to amorphous or paracrystalline material and containing a higher proportion of surface chains (Figs. 5, 8). The crystallinity threshold is probably due to the slower kinetics induced by a higher viscosity or to a

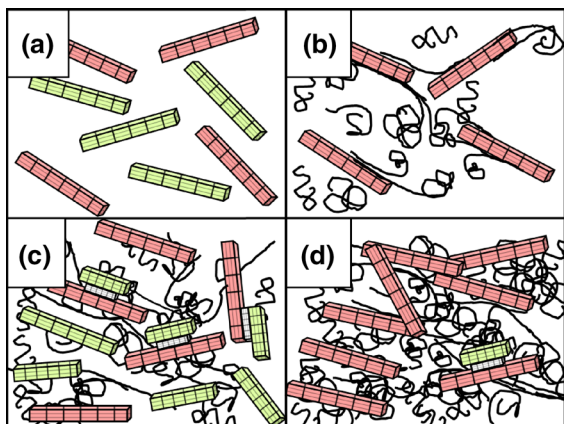


**Fig. 8** **a** The CNC suspension contains both cellulose I (red) and cellulose II (green) nanocrystals. **b** The cellulose II nanocrystals are dissolved during manufacturing and physical adsorption occurs between the cellulose chains in solution (black random coils) and the remaining CNC. At low concentrations, a large amount of cellulose II is cocrystallised (c). In contrast, cellulose II crystallisation is hindered at high concentrations while a percolated and stratified microstructure is favoured (d). (Color figure online)

confinement effect prohibiting chain uncoiling, alignment and periodical packing.

Another effect could shed the light on the particularly low cellulose II content found in ACC8. Assuming a length of  $\sim 105$  nm (TEM data), a width and thickness of  $\sim 5$  nm (AFM and TEM data), a density of 1.6 and a remaining undissolved CNC concentration of  $0.59 \times 0.04 \sim 2.36$  % (XRD data) over the whole volume of solvent, the CNC studied here occupy an hydrodynamic diameter of  $\sim 70$  nm. Their percolation ratio is of  $0.7/(105/5) \sim 3.3$  % (Capadona et al. 2008). The calculated percolation concentration is very close to the actual suspension concentration assuming full cellulose II CNC dissolution, which is a somewhat conservative estimate. The hydrodynamic diameter is also lower than the average CNC length. These figures are such that CNC percolation has probably started to occur, thereby strongly limiting any possible cellulose II growth on the remaining cellulose I templates.

All these results fit nicely with the observed mechanical behaviour of the composites when exposed to humidity. The plasticising effect of moisture comes from the ability of water to intercalate between the weak hydrogen bonds that form the intermolecular bonds between the non-crystallised polymer chains, between the percolated CNC and

possibly between a fraction of non-crystallized tethered chains and CNC (Capadona et al. 2008; Newman 2004; Salmén and Back 1977; Zhou et al. 2001). As a consequence, a well crystallised regenerated cellulosic material is known to be little affected by exposure to water as water cannot penetrate the crystallites. The storage modulus drop upon exposure to humidity is thus expected to be the strongest in the least crystalline composites, which is the case here. However, the more crystalline materials should also be stiffer, in opposition with our RH-DMA measurements. The percolation hypothesis is useful in clarifying this paradoxical observation. Indeed, by assuming a percolated network of CNC in the ACC with the highest initial concentrations (Fig. 8), one can understand their apparent higher stiffness (and brittleness). Since the percolation between CNC is mediated by intermolecular hydrogen bonds, it is also highly susceptible to moisture uptake, which also explains why the stiffer composites undergo the most extensive plasticisation.

Another attention-grabbing feature of the ACC composites produced with the higher CNC concentration is shown by the presence of some unusually sharp XRD peaks (Fig. 2), reflecting a crystallographic texture, or preferential orientation. This microstructure is of particular interest in that the CNC are elongated particles which potentially self-organized in the matrix, thereby creating a seemingly orthotropic material. This statement needs to be backed up by further experimental evidence.

## Conclusions

All-cellulose nanocomposites were successfully made by precipitation and recrystallisation of dissolved cellulose in an ionic liquid/DMSO containing dispersed undissolved CNC. It was shown that these CNC could act as a template and promote the cocrystallisation of cellulose II in the matrix. This cocrystallisation was followed by XRD and by a relative measurement (LOI) of the FTIR  $-\text{CH}$  band over a signal assigned to the hydroxymethyl carbon of the crystalline species, a band known for its sensitivity to local changes. Both demonstrated that an excessive CNC concentration hindered cellulose II recrystallisation. This counter-effect could be attributed to unfavourable kinetics (viscosity) or to a percolation-related confinement. The deduced percolation is also

useful to explain the higher stiffness of the least crystalline composites despite the larger susceptibility of their storage modulus upon exposure to humidity. This result opens perspectives for applications to these bio-based and biodegradable nanocomposites as humidity-responsive ecomaterials such as humidity-controlled dampers. The plasticisation of the percolated network is reversible upon drying, opening interesting shaping opportunities for such films (Capadona et al. 2008; Pullawan et al. 2013). They could thus be produced in a standard form and then stretched after wetting in order to give them a specific shape. A future work will be aimed at gaining an insight in the rheology of cellulose solutions bearing cellulose nanocrystals at different concentration regimes and for CNC of various aspect ratios, as well as looking at the templating effect when the slurry is stretched during regeneration and drying. Another work will more explicitly look at the shape-memory characteristics of these composites.

**Acknowledgments** The authors would like to thank Emilie Perrin (BIA) for her help with the TEM. Financial support from the CNRS was provided through a PEPS grant (BioMIMCellwall). BD would like to dedicate this article to the memory of the late Dr Roger H. Newman.

## References

- Altaner CM, Horikawa Y, Sugiyama J, Jarvis MC (2014) Cellulose  $I_{\beta}$  investigated by IR-spectroscopy at low temperatures. *Cellulose* 21:3171–3179. doi:10.1007/s10570-014-0360-x
- Boerstael H (2006) Liquid crystalline solutions of cellulose in phosphoric acid for preparing cellulose yarns. University of Groningen. <http://www.narcis.nl/publication/RecordID/oai:ub.rug.nl:dbi%2F43da2b779a30f>
- Boluk Y, Lahiji R, Zhao L, McDermott MT (2011) Suspension viscosities and shape parameter of cellulose nanocrystals (CNC). *Colloids Surf Physicochem Eng Asp* 377:297–303. doi:10.1016/j.colsurfa.2011.01.003
- Bras J (2004) Etudes des propriétés barrières de dérivés cellulosiques: application au gel de cellulose du papier sulfuré. Toulouse, INPT
- Buleon A, Chanzy H (1980) Single crystals of cellulose IVII: preparation and properties. *J Polym Sci Polym Phys Ed* 18:1209–1217. doi:10.1002/pol.1980.180180604
- Buleon A, Chanzy H, Roche E (1976) Epitaxial crystallization of cellulose II on valonia cellulose. *J Polym Sci Polym Phys Ed* 14:1913–1916. doi:10.1002/pol.1976.180141016
- Buleon A, Chanzy H, Roche E (1977) Shish kebab-like structures of cellulose. *J Polym Sci Polym Lett Ed* 15:265–270. doi:10.1002/pol.1977.130150502
- Capadona JR, Shanmuganathan K, Tyler DJ et al (2008) Stimuli-responsive polymer nanocomposites inspired by the sea cucumber dermis. *Science* 319:1370–1374. doi:10.1126/science.1153307
- Carillo F, Colom X, Suñol JJ, Saurina J (2004) Structural FTIR analysis and thermal characterisation of lyocell and viscose-type fibres. *Eur Polym J* 40:2229–2234
- Cartier N, Escaffre P, Mathevet F, et al. (1994) Structure and recycling of vegetable parchment. *Tappi J* 77:95–100
- Courtenay W (1878) Improvement in processes of treating vegetable fibrous substances. US 217,448 A
- Duchemin B (2008) Structure, property and processing relationships of all-cellulose composites. Ph.D. Thesis, University of Canterbury
- Duchemin B, Newman R, Staiger M (2007) Phase transformations in microcrystalline cellulose due to partial dissolution. *Cellulose* 14:311–320
- Duchemin BJC, Mathew AP, Oksman K (2009a) All-cellulose composites by partial dissolution in the ionic liquid 1-butyl-3-methylimidazolium chloride. *Compos Part Appl Sci Manuf* 40:2031–2037. doi:10.1016/j.compositesa.2009.09.013
- Duchemin BJC, Newman RH, Staiger MP (2009b) Structure–property relationship of all-cellulose composites. *Compos Sci Technol* 69:1225–1230
- Duchemin BJC, Staiger MP, Tucker N, Newman RH (2010) Aerocellulose based on all-cellulose composites. *J Appl Polym Sci* 115:216–221. doi:10.1002/app.31111
- Duchemin B, Thuault A, Vicente A et al (2012) Ultrastructure of cellulose crystallites in flax textile fibres. *Cellulose* 19:1837–1854. doi:10.1007/s10570-012-9786-1
- Fernandes AN, Thomas LH, Altaner CM et al (2011) Nanostructure of cellulose microfibrils in spruce wood. *Proc Natl Acad Sci USA* 108:E1195–E1203. doi:10.1073/pnas.1108942108
- Fink H-P, Ganster J, Lehmann A (2014) Progress in cellulose shaping: 20 years industrial case studies at Fraunhofer IAP. *Cellulose* 21:31–51. doi:10.1007/s10570-013-0137-7
- Flandin L, Cavaillé JY, Bidan G, Brechet Y (2000) New nanocomposite materials made of an insulating matrix and conducting fillers: processing and properties. *Polym Compos* 21:165–174. doi:10.1002/pc.10174
- Gindl W, Keckes J (2005) All-cellulose nanocomposite. *Polymer* 46:10221–10225
- Goldberg RN, Schliesser J, Mittal A et al (2015) A thermodynamic investigation of the cellulose allomorphs: cellulose (am), cellulose  $I_{\beta}$  (cr), cellulose II (cr), and cellulose III (cr). *J Chem Thermodyn* 81:184–226. doi:10.1016/j.jct.2014.09.006
- Graenacher C (1934) Cellulose solution. US 1943176 A
- Haverhals LM, Reichert WM, Long HCD, Trulove PC (2010) Natural fiber welding. *Macromol Mater Eng* 295:425–430. doi:10.1002/mame.201000005
- Haverhals LM, Sulpizio HM, Fayos ZA et al (2012) Process variables that control natural fiber welding: time, temperature, and amount of ionic liquid. *Cellulose* 19:13–22. doi:10.1007/s10570-011-9605-0
- He X, Xiao Q, Lu C et al (2014) Uniaxially aligned electrospun all-cellulose nanocomposite nanofibers reinforced with cellulose nanocrystals: scaffold for tissue engineering. *Biomacromolecules* 15:618–627. doi:10.1021/bm401656a
- Huber T, Müssig J, Curnow O et al (2012) A critical review of all-cellulose composites. *J Mater Sci* 47:1171–1186. doi:10.1007/s10853-011-5774-3

- Hurtubise FG, Krassig H (1960) Classification of fine structural characteristics in cellulose by infrared spectroscopy. Use of potassium bromide pellet technique. *Anal Chem* 32: 177–181
- Imai T, Sugiyama J (1998) Nanodomains of I $\alpha$  and I $\beta$  cellulose in algal microfibrils. *Macromolecules* 31:6275–6279
- Isogai A (1989) Solid-state CP/MAS <sup>13</sup>C NMR study of cellulose polymorphs. *Macromolecules* 22:3168–3172
- Kalka S, Huber T, Steinberg J et al (2014) Biodegradability of all-cellulose composite laminates. *Compos Part Appl Sci Manuf* 59:37–44. doi:10.1016/j.compositesa.2013.12.012
- Koenig JL (1999) Spectroscopy of polymers. Elsevier, Amsterdam
- Kondo T, Sawatari C (1996) A fourier transform infra-red spectroscopic analysis of the character of hydrogen bonds in amorphous cellulose. *Polymer* 37:393–399
- Liebert TF (2010) Cellulose solvents—remarkable history, bright future. In: Liebert T, Heinz TJ, Edgar KJ (eds) Cellulose solvents: for analysis, shaping and chemical modification, ACS symposium series, vol 1033. American Chemical Society, Washington, DC, pp 3–54
- Lu A, Hemraz U, Khalili Z, Boluk Y (2014) Unique viscoelastic behaviors of colloidal nanocrystalline cellulose aqueous suspensions. *Cellulose* 21:1239–1250. doi:10.1007/s10570-014-0173-y
- Ma H, Zhou B, Li H-S et al (2011) Green composite films composed of nanocrystalline cellulose and a cellulose matrix regenerated from functionalized ionic liquid solution. *Carbohydr Polym* 84:383–389. doi:10.1016/j.carbpol.2010.11.050
- Magalhães WLE, Cao X, Lucia LA (2009) Cellulose nanocrystals/cellulose core-in-shell nanocomposite assemblies. *Langmuir* 25:13250–13257. doi:10.1021/la901928j
- Manabe S, Iwata M, Kamide K (1986) Dynamic mechanical absorptions observed for regenerated cellulose solids in the temperature range from 280 to 600 K. *Polym J* 18:1–14
- Maréchal Y, Chanzy H (2000) The hydrogen bond network in I $\beta$  cellulose as observed by infrared spectrometry. *J Mol Struct* 523:183–196
- Mazeau K (2015) The hygroscopic power of amorphous cellulose: a modeling study. *Carbohydr Polym* 117:585–591. doi:10.1016/j.carbpol.2014.09.095
- Nelson ML, O'Connor RT (1964a) Relation of certain infrared bands to cellulose crystallinity and crystal lattice types. Part II. A new infrared ratio for estimation of crystallinity in celluloses I and II. *J Appl Polym Sci* 8:1325–1341
- Nelson ML, O'Connor RT (1964b) Relation of certain infrared bands to cellulose crystallinity and crystal lattice types. Part I. Spectra of lattice types I, II, III and of amorphous cellulose. *J Appl Polym Sci* 8:1311–1324
- Newman RH (2004) Carbon-13 NMR evidence for cocrystallisation of cellulose as a mechanism for hornification of bleached kraft pulp. *Cellulose* 11:45–52. doi:10.1023/B:CELL.0000014768.28924.0c
- Newman RH (2008) Simulation of X-ray diffractograms relevant to the purported polymorphs cellulose IVI and IVII. *Cellulose* 15:769–778. doi:10.1007/s10570-008-9225-5
- Nishino T, Arimoto N (2005) All-cellulose composite by partial dissolving of fibers. Stockholm
- Nishino T, Matsuda I, Hirao K (2004) All-cellulose composite. *Macromolecules* 37:7683–7687
- Nissan AH, Sternstein SS (1962) Cellulose as a viscoelastic material. *Pure Appl Chem* 5:131–146
- O'Connor RT, DuPré EF, Mitcham D (1958) Applications of infrared absorption spectroscopy to investigations of cotton and modified cottons. *Text Res J* 28:382–392. doi:10.1177/004051755802800503
- Oh SY, Yoo DI, Shin Y et al (2005a) Crystalline structure analysis of cellulose treated with sodium hydroxide and carbon dioxide by means of X-ray diffraction and FTIR spectroscopy. *Carbohydr Res* 340:2376–2391
- Oh SY, Yoo DI, Shin Y, Seo G (2005b) FTIR analysis of cellulose treated with sodium hydroxide and carbon dioxide. *Carbohydr Res* 340:417–428
- Olszewska AM, Kontturi E, Laine J, Österberg M (2013) All-cellulose multilayers: long nanofibrils assembled with short nanocrystals. *Cellulose* 20:1777–1789. doi:10.1007/s10570-013-9949-8
- Oujai S, Shanks RA (2009) Preparation, structure and mechanical properties of all-hemp cellulose biocomposites. *Compos Sci Technol* 69:2119–2126. doi:10.1016/j.compscitech.2009.05.005
- Pinkert A, Marsh KN, Pang S, Staiger MP (2010) Ionic liquids and their interaction with cellulose. *Chem Inform*. doi:10.1002/chin.201017232
- Pullawan T, Wilkinson AN, Eichhorn SJ (2010) Discrimination of matrix–fibre interactions in all-cellulose nanocomposites. *Compos Sci Technol* 70:2325–2330. doi:10.1016/j.compscitech.2010.09.013
- Pullawan T, Wilkinson AN, Eichhorn SJ (2012) Influence of magnetic field alignment of cellulose whiskers on the mechanics of all-cellulose nanocomposites. *Biomacromolecules* 13:2528–2536
- Pullawan T, Wilkinson AN, Eichhorn SJ (2013) Orientation and deformation of wet-stretched all-cellulose nanocomposites. *J Mater Sci* 48:7847–7855. doi:10.1007/s10853-013-7404-8
- Pullawan T, Wilkinson AN, Zhang LN, Eichhorn SJ (2014) Deformation micromechanics of all-cellulose nanocomposites: comparing matrix and reinforcing components. *Carbohydr Polym* 100:31–39. doi:10.1016/j.carbpol.2012.12.066
- Qi H, Cai J, Zhang L, Kuga S (2009) Properties of films composed of cellulose nanowhiskers and a cellulose matrix regenerated from alkali/urea solution. *Biomacromolecules* 10:1597–1602. doi:10.1021/bm9001975
- Rinaldi R (2011) Instantaneous dissolution of cellulose in organic electrolyte solutions. *Chem Commun* 47:511. doi:10.1039/c0cc02421j
- Röder T, Moosbauer J, Kliba G et al (2009) Comparative characterisation of man-made regenerated cellulose fibres. *Lenzing Ber* 87:98–105
- Salmén NL, Back EL (1977) The influence of water on the glass transition temperature of cellulose. *Tappi* 60:137–140
- Schmidt A (1871) Improvement in treating paper and vegetable fibrous substances. US 113,454. Pittsburgh, PA
- Schwanninger M, Rodrigues JC, Pereira H, Hinterstoisser B (2004) Effects of short-time vibratory ball milling on the shape of FT-IR spectra of wood and cellulose. *Vib Spectrosc* 36:23–40
- Sèbe G, Ham-Pichavant F, Ibarboure E et al (2012) Supramolecular structure characterization of cellulose II

- nanowhiskers produced by acid hydrolysis of cellulose I substrates. *Biomacromolecules* 13:570–578. doi:[10.1021/bm201777j](https://doi.org/10.1021/bm201777j)
- Segal L, Creely JJ, Martin AE, Conrad CM (1959) An empirical method for estimating the degree of crystallinity of native cellulose using the X-ray diffractometer. *Text Res J* 29:786–794
- Smole MS, Peršin Z, Kreže T et al (2003) X-ray study of pre-treated regenerated cellulose fibres. *Mat Res Innov* 7:275–282
- Song H, Niu Y, Yu J et al (2013) Preparation and morphology of different types of cellulose spherulites from concentrated cellulose ionic liquid solutions. *Soft Matter* 9:3013–3020. doi:[10.1039/C3SM27320B](https://doi.org/10.1039/C3SM27320B)
- Soykeabkaew N, Arimoto N, Nishino T, Peijs T (2008) All-cellulose composites by surface selective dissolution of aligned ligno-cellulosic fibres. *Compos Sci Technol* 68:2201–2207
- Soykeabkaew N, Nishino T, Peijs T (2009a) All-cellulose composites of regenerated cellulose fibres by surface selective dissolution. *Compos Part Appl Sci Manuf* 40:321–328
- Soykeabkaew N, Sian C, Gea S et al (2009b) All-cellulose nanocomposites by surface selective dissolution of bacterial. *Cellulose* 16:435–444. doi:[10.1007/s10570-009-9285-1](https://doi.org/10.1007/s10570-009-9285-1)
- Sukhov DA, Derkacheva O, Kazanskii SA (1998) Allomorphism of native celluloses by FTIR spectroscopy. In: 5th European workshop on lignocellulosics and pulp. *Advances in lignocellulosics chemistry for ecologically friendly pulping and bleaching technologies*. Aveiro, Portugal, pp 5–66
- Sundberg J, Toriz G, Gatenholm P (2013) Moisture induced plasticity of amorphous cellulose films from ionic liquid. *Polymer* 54:6555–6560. doi:[10.1016/j.polymer.2013.10.012](https://doi.org/10.1016/j.polymer.2013.10.012)
- Takahashi M, Ookubo M (1993) CP/MAS <sup>13</sup>C NMR and WAXS studies on the effects of starting cellulose materials on transition between cellulose polymorphs. *Kobunshi Ronbunshu* 51:107–113
- Takayanagi M, Uemura S, Minami S (1964) Application of equivalent model method to dynamic rheo-optical properties of crystalline polymer. *J Polym Sci Part C Polym Symp* 5:113–122. doi:[10.1002/polc.5070050111](https://doi.org/10.1002/polc.5070050111)
- Wang Y, Chen L (2010) Impacts of nanowhisker on formation kinetics and properties of all-cellulose composite gels. *Carbohydr Polym* 83:1937–1946. doi:[10.1016/j.carbpol.2010.10.071](https://doi.org/10.1016/j.carbpol.2010.10.071)
- Wang S, Cheng Q (2009) A novel process to isolate fibrils from cellulose fibers by high-intensity ultrasonication, Part 1: process optimization. *J Appl Polym Sci* 113:1270–1275. doi:[10.1002/app.30072](https://doi.org/10.1002/app.30072)
- Wang L, Gao L, Cheng B et al (2014) Rheological behaviors of cellulose in 1-ethyl-3-methylimidazolium chloride/dimethyl sulfoxide. *Carbohydr Polym* 110:292–297. doi:[10.1016/j.carbpol.2014.03.091](https://doi.org/10.1016/j.carbpol.2014.03.091)
- Zhou S, Tashiro K, Hongo T et al (2001) Influence of water on structure and mechanical properties of regenerated cellulose studied by an organized combination of infrared spectra, X-ray diffraction, and dynamic viscoelastic data measured as functions of temperature and humidity. *Macromolecules* 34:1274–1280. doi:[10.1021/ma001507x](https://doi.org/10.1021/ma001507x)
- Zhu S, Wu Y, Chen Q et al (2006) Dissolution of cellulose with ionic liquids and its application: a mini-review. *Green Chem* 8:325–327
- Zugenmaier P (2001) Conformation and packing of various crystalline cellulose fibers. *Prog Polym Sci* 26:1341–1417